# Composition and Temperature Dependence of Electronic and Optical Properties in Manganese Doped Tin Dioxide Films on Quartz Substrates Prepared by Pulsed Laser Deposition

**W. W. Li,[†] J. J. Zhu,[†] J. D. Wu,[‡] J. Sun,[‡] M. Zhu,[§] Z. G. Hu,*[,†] and J. H. Chu[†]**

Key Laboratory of Polar Materials and Devices, Ministry of Education, Department of Electronic Engineering, East China Normal University, Shanghai 200241, People's Republic of China, Key Laboratory for Advanced Photonic Materials and Devices, Ministry of Education, Department of Optical Science and Engineering, Fudan University, Shanghai 200433, People's Republic of China, and Department of Physics, Shanghai Jiao Tong University, Shanghai 200240, People's Republic of China

**ABSTRACT** Manganese-doped tin dioxide ($SnO_2$:Mn) films (grain size of about 16 nm) with different composition $x$ from 2.5 to 15% have been grown on quartz substrates by pulsed laser deposition. X-ray diffraction analysis show that the films are polycrystalline and an impurity phase appears until the $x$ is up to 15%. The optical functions in the photon energy range of 0.5−6.5 eV have been extracted by fitting the transmittance spectra at room temperature with the Adachi's dielectric function model (Adachi, S. *Phys. Rev. B* **1987**, *35*, 7454). The refractive index generally decreases with the doping composition except for the film doped with 15% Mn because of the variation in crystalline formation and electronic energy band structure. Because of the repelling effect of 2p−3d hybridization and its perturbation on O 2p-like bands, the optical band gap linearly decreases and can be well expressed by (4.26−3.8$x$) eV. The transmittance spectra of the film doped with 2.5% Mn at the temperature varied from 5.3 to 300 K have been recorded and a redshift trend of the absorption edge with increasing the temperature can be observed. The results indicate that the dielectric functions decrease with the temperature at the photon energies above the fundamental band gap. Moreover, the optical band gap is shrinked from 4.30 to 4.20 eV with increasing the temperature because of the modification of the electron−phonon interactions. The band gap narrowing coefficient of the $SnO_2$:Mn film with 2.5% Mn is estimated to be about $-5.74 \times 10^{-4}$ eV/K at room temperature.

**KEYWORDS:** $SnO_2$:Mn • optical properties • temperature dependence • pulsed laser deposition

## 1. INTRODUCTION

The idea of utilizing the spin of carriers in novel spintronic devices has led to efforts in fabricating and investigating appropriate new semiconductor materials during the past years. Diluted magnetic semiconductors (DMS) have attracted considerable interest because of their potential applications in spinelectronic, optoelectronic, and magnetoelectronic devices (1−5). Recently, many investigations have been focused on 3d transition metals (TM) doped wide-band gap oxide semiconductors, such as tin dioxide ($SnO_2$) (1), zinc oxide (ZnO) (6), and titanium dioxide ($TiO_2$) (7). These materials were amplified by the theoretical predictions, suggesting that ferromagnetism (FM) with Curie temperatures above room temperature (RT) could be obtained (8−11). In particular, $SnO_2$ offers a unique combination of large optical band gap (OBG), excellent optical transparency, metal-like conductivity, easy doping, and high chemical stability, which make it promising as an alternative host materials for DMS and is technologically used as a transparent electrode in solar cells (12, 13). Many research groups have reported magnetic, electrical, and optical properties for various kinds of TM-doped $SnO_2$, such as vanadium(V), manganese (Mn), iron (Fe), and cobalt (Co) (1−4). Among them, Mn element is a typical TM, which is often used as a spin injector, yielding giant magnetoresistance and magneto-optical effect. Mn-doped $SnO_2$ ($SnO_2$:Mn) is experimentally reported to be paramagnetic and shows large magnetoresistance (1). The doping of Mn could provide the influence on the distribution of oxygen vacancy and further affect the magnetic properties of $SnO_2$:Mn films (4). It indicates that the Mn incorporation can result in the electronic band structure variation of $SnO_2$ host crystal. On the other hand, it is well-known that films can be deposited directly on diversified substrates and are expected to yield better sensitivity and faster response than the equivalent bulk single crystal. Hence, it is significant to further investigate the physical properties of $SnO_2$:Mn films.

As we know, the physical properties of films are strongly dependent on the experimental conditions: substrate, growth

* Corresponding author. E-mail: zghu@ee.ecnu.edu.cn.
Received for review April 21, 2010 and accepted July 7, 2010
[†] East China Normal University.
[‡] Fudan University.
[§] Shanghai Jiao Tong University.
DOI: 10.1021/am100353f

technique, crystalline quality, intrinsic defects, and doping elements (14, 15). Many fabrication techniques are currently applied to prepare $SnO_2$:Mn films such as pulsed laser deposition (PLD) (1), spray pyrolysis (2), and sol−gel method (5). Among them, the PLD is a well-adopted method because of its evident advantages such as high quality of film, composition control, and uniformity (14). In particular, based on the precondition of the known composition in the targets, the precise composition could be more easily controlled by the PLD technique. On the other hand, the optical constants play an important role in the optoelectronic device design. For example, energy transport by exciton and performance of luminescent devices depend on the dielectric constant of the concerned material (16). Furthermore, macroscopical dielectric functions, which can be related to the electronic band structure of materials, not only provide basic optical properties but will also be critical for developing the novel materials for optoelectronic applications (10, 17). Unfortunately, there are few reports about electronic and optical properties of $SnO_2$:Mn films on the transparent substrates in a wider photon energy region. Kimura et al. found that the absorption edge of PLD-derived $SnO_2$:Mn films on sapphire substrates redshift as the Mn composition $x$ ($C_{Mn}$) (1). Gopinadhan et al. suggested that the OBG of $SnO_2$:Mn films, which were prepared by spray pyrolysis technique on quartz substrates, shows no systematical change with the $C_{Mn}$ (2). However, no more detailed electronic and optical properties of the $SnO_2$:Mn films have been presented, especially for dielectric functions and TM doping effects. Taking into account that the electronic and optical properties of films strongly depend on substrate materials, doping composition, and deposition methods, Mn doping effects on the dielectric functions and OBG energy of $SnO_2$:Mn films still remain as an open issue. The composition dependence of optical properties plays an important role in design, optimization, and evaluation of DMS-based optoelectronic and spinelectronic devices. Therefore, the dielectric functions of $SnO_2$:Mn films in a wider photon energy range should be thoroughly studied in order to exploit its potential applications.

Temperature dependence of electronic and optical properties in semiconductor materials is of fundamental importance in many optoelectronic applications. For example, a part of the laser power is absorbed by material when it is used in laser applications, and then the material is heated and ultimate refractive index of the medium is changed (18). As for the applied science standpoint, accurate knowledge of the variations of the refractive index with the temperature is important among other things for designing solar energy converters (19). Therefore, temperature-induced deviations of the optical constants from the value measured at RT is of considerable interest for the optical materials, which are commonly used in the fabrication of optoelectronic devices. It is desirable to carry out a delicate study regarding these essential properties of $SnO_2$:Mn material. There are some spectral techniques to determine optical constants of film materials. Note that transmittance spectra is a nondestructive probe technique, which can directly provide OBG, optical constants, absorption characteristics, band tail state behavior, and optical phonon modes, etc. (20). It should be emphasized that the transmittance technique is widely acceptable and applied in the case of transparent substrates, which can directly present the transmission and/or absorption of material system studied. It is easy and useful to derive the dielectric functions of films by subtracting the contributions from transparent substrates.

In this article, the fabrication and structure of $SnO_2$:Mn films with different $C_{Mn}$ (from 2.5 to 15%) deposited on quartz substrates have been studied. The dielectric functions of the films from ultraviolet (UV) to near-infrared (NIR) photon energy region and its composition and temperature dependences have been investigated by spectral transmittance technique. A dielectric function theoretical model is presented to reproduce the experimental transmittance spectra well. The influences from the $C_{Mn}$ and temperature on the electronic band structure have been discussed in detail.

## 2. EXPERIMENTAL SECTION

**Growth of the $SnO_2$:Mn Films.** The $SnO_2$:Mn targets in the diameter of 3 cm were prepared using a conventional solid-state reaction sintering (21). During the preparation, MnO powder was mixed with $SnO_2$ powder (99.99%) in which Mn mole fraction was varied as 2.5, 5, 7.5, 10, 12.5, and 15%, respectively. Double-side polished quartz wafers, which were selected for the UV transmittance measurements, were used as the substrates. The substrates were rigorously cleaned in pure ethanol with an ultrasonic bath and were rinsed several times by deionized water. The wafers were dried in a pure nitrogen stream before the deposition of the films. The $SnO_2$:Mn films with the nominal thickness of about 200 nm were grown by the PLD. The growth chamber was first pumped down to a base pressure of $1 \times 10^{-4}$ Pa. A Q-switched pulse Nd:YAG (yttrium aluminum garnet) laser (532 nm wavelength, 5 ns duration), which works at repetition rate of 10 Hz and energy of 40 mJ/pulse, was used for target ablation. The film was grown immediately after the target was preablated. The distance between the target and the substrate was kept at 3 cm and the deposition time was set to about 30 min. Then the films were annealed at 900 °C in an oxygen ambience by a rapid thermal annealing process. A detailed preparation of the films can be found in refs 14 and 22. It should be noted that the PLD technique can easily control the doping composition of the $SnO_2$:Mn films, which should not show a large deviation from the stoichiometric ratio in the targets. Moreover, the previous results indicate that the composition error for oxide semiconductor films was found to be located in about ±0.1% by X-ray photoelectron spectroscopy (XPS) in the present PLD method applied (22). Thus, it is reasonable that the $C_{Mn}$ confidence limit of the present $SnO_2$:Mn films is similar to the above case and estimated to be about ±0.1%, which is small and can be neglected, as compared to the doping composition.

**XRD and Transmittance Spectral Measurements.** The crystalline structure of the $SnO_2$:Mn films was analyzed by X-ray diffraction (XRD) using Cu $K\alpha$ radiation (D/MAX-2550 V, Rigaku Co.). In the XRD experiments, a vertical goniometer (model RINT2000) was used, and continuous scanning mode ($2\theta/\theta$) was selected with an interval of 0.02° and the scanning rate is 10°/min. The optical transmittance at RT were recorded with a double beam ultraviolet-infrared spectrophotometer (PerkinElmer Lambda 950) at the photon energy from 0.5 to 6.5 eV (190−2650 nm) with a spectral resolution of 2 nm. The trans-

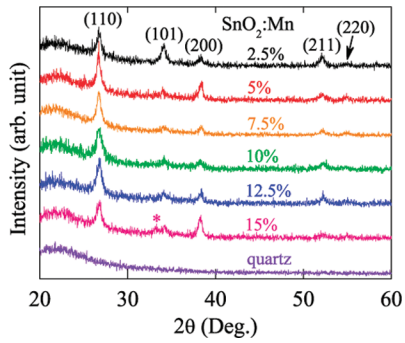


**FIGURE 1. XRD patterns of the $SnO_2$:Mn films with different Mn composition and quartz substrate. Note that the label (*) denotes the diffraction peak (222) at about 33.2° from $Mn_2O_3$ for the film doped with the Mn composition of 15%.**

mittance spectrum of double-side polished quartz substrate was measured in order to derive its dielectric functions. The 2.5% Mn-doped $SnO_2$ ($Sn_{0.975}Mn_{0.025}O_2$) film was mounted into an optical cryostat (Janis SHI-4−1) and the transmittance spectra at different temperature from 5.3 to 300 K were measured using the same spectrophotometer. It is noted that the interval of temperature is 10 K and about 25 K for the temperature region of 5.3−100 K and 100−300 K, respectively. To eliminate the effects from the windows of cryostat, the transmittance spectra of the quartz windows were also recorded at corresponding temperature. It should be emphasized that no mathematical smoothing has been performed on the experimental data.

## 3. RESULTS AND DISCUSSION

**Structural Analysis.** The XRD patterns of the films with the $C_{Mn}$ from 2.5 to 15% and the quartz substrate have been shown in Figure 1. As can be seen, there are the diffraction peaks (110), (101), (200), (211), and (220) and the quartz substrate is amorphous with a broadening peak near 22°. Therefore, it can be concluded that the diffraction peaks observed can be derived from the $SnO_2$:Mn films, suggesting that they are polycrystalline with different orientations. Note that the (101) peaks of the films show a weak diffraction intensity except for the film doped with 2.5% Mn, which may be ascribed to the dopant contributions. It indicates that the higher $C_{Mn}$ could result in the different crystalline formation. In addition, the increasing crystalline defects could be another possible cause. It can be confirmed by the transmittance results, where the fundamental absorption edges become more flat except for the film doped with 2.5% Mn. Note that the diffraction pattern of the film doped with 15% Mn displays a weak undesired peak (labeled by *) at about 33.2°, which could be assigned to the diffraction peak (222) from the $Mn_2O_3$ material. It suggests that the impurity phase appears until the $C_{Mn}$ is up to 15%. The similar phenomenon has been found by Xiao et al. for the $SnO_2$:Mn sample doped with about 11% Mn (5). Therefore, one can conclude that the Sn lattice position is partly occupied by the Mn dopant and the replacement is indeed realized in the $SnO_2$ matrix. The grain size $r$ can be calculated from the (110) diffraction peak according to the well-known Scherrer equation $r = K\lambda/\beta \cos\theta$; here, $K \approx 1$ is the shape factor, $\lambda = 1.540$ Å is the average wavelength of Cu $K\alpha$ radiation, $\beta$ is the full width at half-maximum, and $\theta$ is the diffraction angle. The average grain size is estimated to about 16 nm for the $SnO_2$:Mn films. The calculated $a$-axis lattice constant for all films is averaged to about 4.715 Å. The value is slightly less than those of the films prepared by spray pyrolysis (about 4.725 Å) (2) and sol−gel method (about 4.726 Å) (5). The discrepancy can be ascribed to different crystallinity, strain, and lattice mismatch with the substrate.

**Theoretical Consideration.** The inverse synthesis method is based on a phenomenological model fitted to the experimental results. The reliability of the inverse synthesis method mainly depend on the validity of the optical model and the fitting statistics. A three-phase layered structure (air/film/substrate) was used to calculate the transmittance spectra of the $SnO_2$:Mn films (23, 24). At the normal incidence configuration, the transmittance coefficient can be described as follows

$$t = \frac{t_{01}t_{12}e^{-i\delta}}{1 + t_{01}t_{12}e^{-2i\delta}} \quad (1)$$

Where the partial transmittance coefficient $t_{01}$ (air−film) and $t_{12}$ (film−substrate) are written as

$$t_{i,i+1} = \frac{2\sqrt{\tilde{\varepsilon}_i}}{\sqrt{\tilde{\varepsilon}_i} + \sqrt{\tilde{\varepsilon}_{i+1}}} \quad (2)$$

The phase factor for the film with thickness $d$ is described by $\delta = 2\pi d(\tilde{\varepsilon}_1)^{1/2}/\lambda$. Here, $\lambda$ is the incident wavelength, and the dielectric function of vacuum, the film, and the substrate are $\tilde{\varepsilon}_0$ (=1), $\tilde{\varepsilon}_1$, and $\tilde{\varepsilon}_2$, respectively. Thus, the spectral transmittance can be readily obtained from $T = \text{Real}[(\tilde{\varepsilon}_2)^{1/2}]tt^*$. Note that the absorption from the substrate must be taken into account to calculate the transmittance of the film−substrate system. Therefore, the total transmittance is given by $T = T_{20}T_f \exp(-\alpha_s)/(1 - R_{20}R_f \exp(-2\alpha_s))$, where $T_{20}$ and $R_{20}$ are the transmittance and reflectance at substrate−air interfaces, respectively. Also, $\alpha_s = 4\pi k_s d_s/\lambda$, $d_s$ is the substrate thickness (0.5 mm) and $k_s$ the extinction coefficient of the substrate, whereas $T_f$ is the overall transmittance from the front side of the film and $R_f$ is the overall reflectance from the back side of the film (25).

It is a challenge to simulate transmittance spectra of semiconductor film in a wider photon energy region because there is a stronger parameter correlation if a complicated dielectric function model is applied (25). For wide band gap semiconductor materials, the dielectric response, which can be described by the contribution from the lowest three-dimensional $M_0$ type critical point (CP), is written as the following Adachi's model

$$\tilde{\varepsilon}(E) = \varepsilon_\infty + \frac{A_0[2 - (1 + \chi_0)^{1/2} - (1 - \chi_0)^{1/2}]}{E_g^{3/2}\chi_0^2} \quad (3)$$

Here, $\chi_0 = (E + i\Gamma)/E_g$, $\varepsilon_\infty$ is the high-frequency dielectric constant, $E_g$ the fundamental optical transition energy (i.e.,

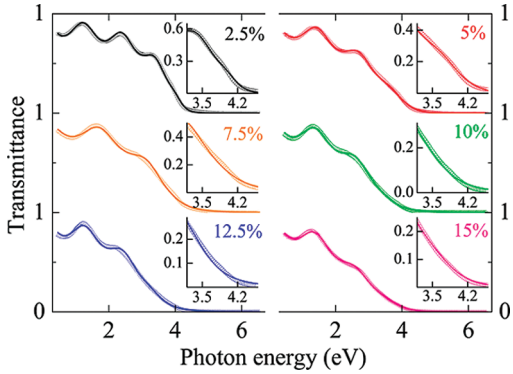


**FIGURE 2. Experimental (dotted lines) and best-fit (solid lines) transmittance spectra of the $SnO_2$:Mn films from ultraviolet to near-infrared photon energy region at room temperature. The insets show an enlarged fitting fundamental band gap region of 3.2−4.6 eV.**

OBG), $E$ the incident photon energy, and $A_0$ and $\Gamma$ the strength and broadening parameters of the $E_g$ transition, respectively (26, 27). It should be emphasized that the above Adachi's model, which abides by the Kramers−Krönig transformation in the entirely measured photon energy region, is successfully applied in many semiconductor and dielectric materials (10, 14, 23). The best-fit model is chosen by optimizing simultaneously the comparison between the experimental and calculated spectra, unbiased estimator for the difference between them, physical likelihood of the solution, 90% confidence limits on each fitting parameter, and correlation coefficient matrix describing the degree of interdependence between the parameters. The deviation parameter $\sigma$ is defined as $\sigma^2 = (1/m)\sum_{i=1}^{m}(T_{exp,i} - T_{cal,i})^2$, here $T_{exp,i}$ and $T_{cal,i}$ are the measured and calculated values at the $i$th data of $m$ photon energy. A least-squares-fitting procedure employing the modified Levenberg−Marquardt algorithm is used in the fitting. The fitting is a process of minimizing $\sigma$ with the optimized values of the fitting parameters (28). It should be emphasized that the dielectric functions of the substrate should be required in order to reproduce the transmittance spectra of the $SnO_2$:Mn/quartz multilayer structures. In the present work, the dielectric function of the quartz substrate is nearly identical to the reported values (29).

**Composition Dependence of UV−NIR Dielectric Functions for the $SnO_2$:Mn Films.** The experimental transmittance spectra of the $SnO_2$:Mn films are plotted in Figure 2 with the dotted lines. The transmittance spectra are similar to those reported by Kimura et al. (1). However, there are fewer interference oscillation periods than in the results presented by Gopinadhan et al. (2) because of a finite film thickness. As compare to undoped $SnO_2$ (3), the decreasing of transmittance intensity shows that the film material becomes opaque as the Mn doping. Nevertheless, the similar results have been also presented in Co- and Fe-doped $SnO_2$ (3). The Fabry−Pérot interference patterns, which are due to the multireflectance between the film and substrate, have been observed in the transparent region. It is worth noting that the fundamental absorption edge becomes much flatter with increasing $C_{Mn}$. It indicates that the Urbach tail states, which can be due to the dopant

**Table 1. Adachi's Parameter Values of the $SnO_2$:Mn Films with Different Mn Composition are Determined from the Simulation of Room Temperature Transmittance Spectra in Figure 2[a]**

| samples | $C_{Mn}$ (%) | thickness $d$ (nm) | $\varepsilon_\infty$ | $A_0$ ($eV^{3/2}$) | $E_g$ (eV) | $\Gamma$ (eV) |
|---|---|---|---|---|---|---|
| A | 2.5 | 258 | 1.68 | 71.0 | 4.20 | 0.33 |
| | | (1) | (0.08) | (2.8) | (0.01) | (0.01) |
| B | 5 | 217 | 1.15 | 97.8 | 4.33 | 0.70 |
| | | (1) | (0.07) | (2.8) | (0.02) | (0.01) |
| C | 7.5 | 182 | 1.99 | 55.1 | 3.89 | 0.68 |
| | | (1) | (0.05) | (1.8) | (0.02) | (0.01) |
| D | 10 | 224 | 2.08 | 47.1 | 3.55 | 0.79 |
| | | (1) | (0.05) | (1.7) | (0.03) | (0.01) |
| E | 12.5 | 247 | 2.24 | 39.2 | 3.45 | 0.75 |
| | | (1) | (0.05) | (1.4) | (0.03) | (0.01) |
| F | 15 | 216 | 0.89 | 104.2 | 4.12 | 1.15 |
| | | (1) | (0.13) | (5.9) | (0.05) | (0.02) |

[a] The 90% reliability of the fitting parameters is given in parentheses.

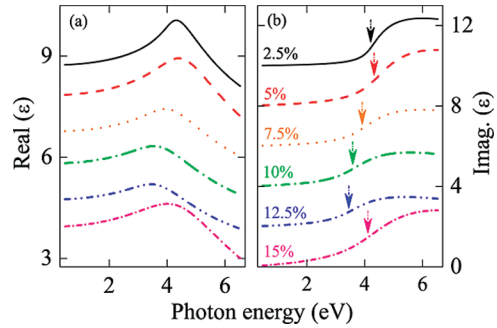


**FIGURE 3. Mn composition effects on the dielectric functions: (a) real part and (b) imaginary part of $SnO_2$:Mn films in the photon energy range of 0.5−6.5 eV. Note that the $\varepsilon_1$ and $\varepsilon_2$ are vertically shifted by adding 1 and 2, respectively. The arrows indicate the energy position of the fundamental optical band gap.**

defects, destruction of the crystal translational symmetry, and/or grain boundary, increase with $C_{Mn}$ (23, 30, 31). The dielectric functions of the $SnO_2$:Mn films can be uniquely determined by fitting the model function to the experimental data. The reproduced transmittance data with the Adachi's model are also plotted in Figure 2 by the solid lines. A good agreement is obtained between the experimental and calculated spectra in the entirely measured photon energy range, especially near the fundamental band gap region (see the insets of Figure 2). The fitted parameter values and film thickness are summarized in Table 1. Note that the film doped with 15% Mn has a minimum $\varepsilon_\infty$ value and a maximum $A_0$ value. It indicates that the film has a mostly transition-energy strength and the contributions from the high-energy electronic transition are slightly remarkable.

The evaluated dielectric functions of the $SnO_2$:Mn films are shown in Figure 3. The evolution of $\tilde{\varepsilon}$ with the photon energy is a typical optical response behavior of dielectric and/or semiconductors (26, 32). Generally, the real part $\varepsilon_1$ increases with the photon energy and approaches the maximum, and then decreases with further increasing photon frequency due to the known Van Hove singularities (26, 32). At the He−Ne laser wavelength of 632.8 nm (1.96

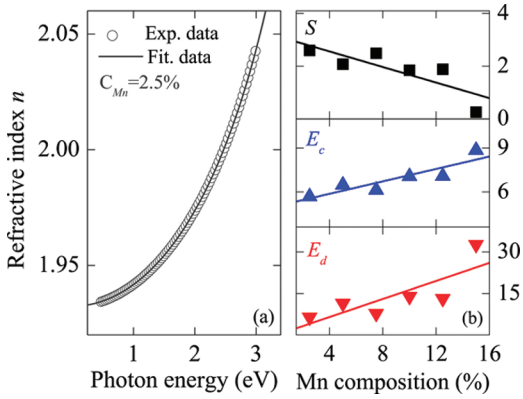


**FIGURE 4. (a) Single oscillator function model in the transparent region for the $SnO_2$:Mn film with the Mn composition of 2.5%. (b) Composition dependence of the oscillator parameters for the $SnO_2$:Mn films. The solid lines are the linear fitting results to guide the eyes.**

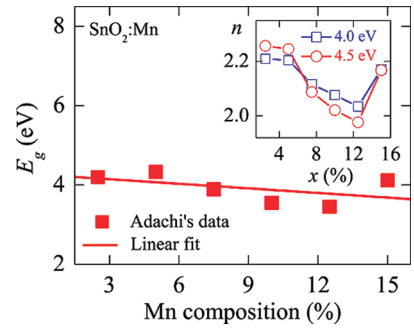


**FIGURE 5. Linearly fitting result of $E_g$ as a function of Mn composition for the $SnO_2$:Mn films. The inset shows the variation of refractive index with the Mn composition at the photon energies of 4.0 and 4.5 eV, respectively.**

eV), the $\varepsilon_1$ value of the $SnO_2$:Mn films was roughly varied from 3.83 to 4.12 with the doping compositions. These values are slightly less than that reported for the films prepared on sapphire substrates (21). It suggests that these films have relatively low packing density. This discrepancy can be ascribed to different substrate, growth technique, and crystalline quality. Note that the peak position of $\varepsilon_1$ approximately shifts toward lower energy side and the intensity generally decreases with the $C_{Mn}$ except for the film doped with 15% Mn. The phenomena can be ascribed to the partial crystalline structure distortion of the films. It could provide the perturbation on the energy band structure and induce the optical response discrepancy. The sharp increasing of the real part in the position and intensity for the film doped with 15% Mn could be attributable to the existence of the $Mn_2O_3$ impurity, which might strengthen the $\varepsilon_1$ value. Note that the phenomena have been confirmed by the XRD patterns, as seen in Figure 1. Moreover, it can be found that the real part of dielectric functions of $Mn_2O_3$ (33) is larger than that of pure $SnO_2$ (34), suggesting that the transition from $SnO_2$ to $Mn_2O_3$ may appear with a higher Mn composition introduction. Thus, the dielectric functions also present the corresponding trend with increasing $C_{Mn}$.

**Electronic Band Structure of the $SnO_2$:Mn Films.** To give an insight on the electronic structure of the $SnO_2$:Mn films, the refractive index $n$ below the fundamental band gap was fitted with a dispersion formula corresponding to a single oscillator function (SOF): $n^2 = S + E_cE_d/(E_c^2 - E^2)$. Here, $S$ is the contribution from high-energy CP transitions, $E_c$ is the oscillator energy, and $E_d$ is the dispersion energy (10). The fitting quality from the $Sn_{0.975}Mn_{0.025}O_2$ film and the parameter values have been exhibited in panels a and b in Figure 4, respectively. The single-oscillator model gives a relatively good description to the optical dispersion in the transparent range. Note that the $S$ value generally decreases with increasing $C_{Mn}$, which indicates that the effects from the high-frequency electronic transitions become less in the $SnO_2$:Mn films. On the other hand, $E_c$ and $E_d$ generally increase with the Mn composition. Note further that the film doped with 15% Mn has a remarkable parameter values because of the co-operation from $Mn_2O_3$ and $SnO_2$:Mn. It can be found that the maximum optical transition occurs near the energy range of 5.3−8.9 eV from the fitted oscillator energy. These values are much larger than the OBG energy of $SnO_2$. It indicates that the optical dispersion in the transparent region is mainly ascribed to the higher CP virtual transitions and not by the fundamental band gap energy, which is similar to the result from other wide band gap oxides (10). It should be emphasized that the SOF formula is valid only in the transparent region and here gives the electronic band structure of the $SnO_2$:Mn films.

The long wavelength refractive index $n(0)$, which is related to the total effective number of valence electrons per atom in materials, can be calculated from $((E_d/E_c) + 1)^{1/2}$. The $n(0)$ is estimated to be about 1.46, 1.66, 1.51, 1.72, 1.69, and 2.16 at zero point with the $C_{Mn}$, which indicates that the dielectric constants $[n^2(0)]$ are 2.14, 2.77, 2.28, 2.97, 2.86, and 4.68, respectively. For theoretically calculating $n(0)$, the $f$-sum-rule integral can be written as $n^2(0) - 1 = (4/\pi)\int_0^\infty (n(\omega')k(\omega')/(\omega'))d\omega'$. It indicates that the long wavelength refractive index is smaller for materials with wide band gap because there is lower energy transition possibility, which results in fewer contributions to the imaginary part of dielectric functions $[n(\omega)k(\omega)]$. As presented in the inset of Figure 5, the $n$ values generally decrease with the $C_{Mn}$ at the photon energy of 4.0 and 4.5 eV except for the film doped with 15% Mn, which indicates that the Mn introduction can result in the smaller refractive index. Again, the abrupt increase of $n$ value for the film doped with 15% Mn could be attributed to the effect from the $Mn_2O_3$ impurity, as discussed previously.

**Mn Effects on the Optical Band Gap of the $SnO_2$:Mn Films.** The absorption edge of $SnO_2$ has been assigned to interband transitions from the valence band edge with O 2p orbitals to the conduction band edge with Sn 5s orbitals (21, 35). The replacement of Sn with Mn cation can affect the hybridization strength between localized $M_n$ 3d states and O 2p valence bands. It will result in the electronic band structure variations of the $SnO_2$:Mn films. The OBG energy for the $SnO_2$:Mn films can be calculated based on Tauc's law by considering a direct transitions between the valence and conduction bands when the photon energy falls on materials. Here, as one of the fitting parameters in the Adachi's model, the OBG can be readily obtained by simulating the

transmittance spectra (see Table 1). From the fitting parameters, the $E_g$ linearly decreases from 4.33 to 3.45 eV corresponding to increasing $C_{Mn}$, which could be well expressed by the form $(4.26-3.8x)$ eV with the $C_{Mn}$ changing from 2.5 to 15%, as seen in Figure 5. It indicates that the absorption edge shifts to a lower-energy side for Mn-doped films, suggesting matrix incorporation of Mn atoms, which are well-known to occur in DMS materials (11). Nevertheless, these values are larger than that reported in ref 2. In the $SnO_2$:Mn films, O ions around Mn ions form an octahedral crystal field, splitting 3d orbitals into lower $t_{2g}$ states and upper $e_g$ states (4). For Mn ions, the three 3d ($t_{2g}$) states are occupied and the other three $t_{2g}$ and four $e_g$ states are empty and located inside the band gap form by Sn 5s- and O 2p-like bands (21). Note that the $C_{Mn}$ increasing can affect the O 2p and Mn 3d orbital distributions, which will induce the $t_{2g}$ and $e_g$ states located at different level in the energy space. It further results in the increasing of oscillator energy, as confirmed by the single oscillator model fitting. Moreover, the filled Mn 3d states are strongly hybrided with the O 2p states, giving a broad band with a width comparable to O 2p states (4). Therefore, the repelling effect of 2p−3d hybridization tends to affect the O 2p-like bands (21), which will further decrease the OBG in the $SnO_2$:Mn films.

**Transmittance Spectra at Different Temperature for the $Sn_{0.975}Mn_{0.025}O_2$ Film.** The temperature effects on the optical properties in the $SnO_2$:Mn films are also crucial for the design of DMS-based optoelectronic and spinelectronic devices. Undoubtedly, the film doped with 2.5% Mn contains the minimum magnetic doping concentration in the present work. It can be expected that the $Sn_{0.975}Mn_{0.025}O_2$ film is of both the typical semiconductor and magnetic properties above room temperature. Therefore, we believe that the $Sn_{0.975}Mn_{0.025}O_2$ film is a good prototype to study the $SnO_2$-based diluted magnetic semiconductors. On the other hand, all films were prepared at the same experimental condition by PLD, which can be used to control the quality and uniformity of the films well. One can expect that the variation trend of the films in electronic and optical properties with the temperature at different Mn composition could be similar. Hence, the film doped with the $C_{Mn}$ of 2.5% was chosen for the temperature dependence studies. For example, the experimental transmittance spectra of the $Sn_{0.975}Mn_{0.025}O_2$ film at 5.3, 80, 150, and 250 K are shown in the inset of Figure 6 with the dotted curves. To obtain the transmittance of the $Sn_{0.975}Mn_{0.025}O_2$ film, we can eliminate the absorption of quartz windows by dividing by the transmittance of the film at the same temperature. It should be emphasized that the absorption of the quartz windows is small. The spectra can be roughly divided into three specific regions: a transparent oscillating one (lable with "I"), a low transmittance one ("II"), and a strong absorption one ("III") at higher photon energies. Note that the absorption edge is near the end of the interference oscillations and located in the photon energy II. The experimental data were also simulated on the basis of the Adachi's model, and the fitting results are plotted in the inset of Figure 6 with the solid

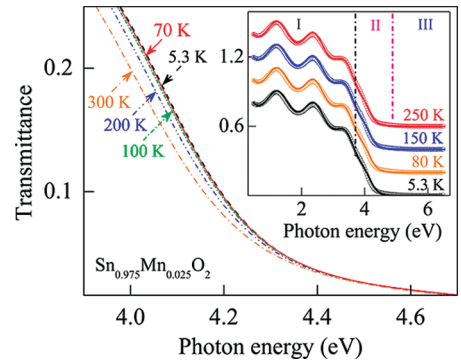


**FIGURE 6. Enlarged band gap region of the film doped with 2.5% Mn at temperatures of 300, 200, 100, 70, and 5.3 K, respectively. The inset shows the experimental (dotted curves) and fitting (solid curves) transmittance spectra at temperatures of 5.3, 80, 150, and 250 K, respectively. Note that the transmittance is vertically shifted by adding 0.2 for clarity.**

curves. The experimental and calculated spectra agree well again in the entirely measured photon energy range. Figure 6 presents the enlarge band gap region of the $Sn_{0.975}Mn_{0.025}O_2$ film at temperatures of 300, 200, 100, 70, and 5.3 K, respectively. It can be clearly observed that the absorption edge shift toward the higher energy side with decreasing the temperature, which agrees with most of the semiconductor materials (36, 37). It suggests that the OBG energy decreases with the temperature and the $Sn_{0.975}Mn_{0.025}O_2$ film has a negative temperature coefficient. However, the shift in the high temperature region (100−300 K) is larger than that in the low temperature region (5.3−100 K) and the total shift of the absorption edge is smaller than other wide band gap materials, such as hexagonal gallium nitride (GaN) (38).

**UV−NIR Dielectric Functions of the $Sn_{0.975}Mn_{0.025}O_2$ Film from 5.3 to 300 K.** The temperature dependence of structure in optical constants is directly related to the temperature dependence of the band states involved in the transition process (19). The fitted parameter values simulating by the Adachi's dielectric function model are summarized in Table 2. Note that the variation of thickness is located within the fitting errors with decreasing the temperature. Hence, the thermal effect on the film thickness can be negligible and the thickness of the film was fixed to 258 nm at RT. It can be found that the $\varepsilon_\infty$ value increases with increasing the temperature. It indicates that the contributions from the high-energy electronic transition for the film increase with the temperature. Moreover, the fact that the parameter $A_0$ decreases with the temperature reveals that the strength of the fundamental optical transition energy becomes remarkable with the temperature. The phenomena can be ascribed to the electronic band structure variations of the film under the lower temperatures. The top panel of Figure 7 depicts the evaluated dielectric functions of the $Sn_{0.975}Mn_{0.025}O_2$ film at the temperatures of 5.3, 150, 200, 250, and 300 K, respectively. At the wide transparent region, both the real part $\varepsilon_1$ and imaginary part $\varepsilon_2$ remain as a constant, which suggests that these values do not connect with the variation of the temperature very much. The peak position of the $\varepsilon_1$, which

**Table 2. Adachi's Parameter Values of the $Sn_{0.975}Mn_{0.025}O_2$ Film at Different Temperatures[a]**

| temperature (K) | $\varepsilon_\infty$ | $A_0$ ($eV^{3/2}$) | $E_g$ (eV) | $\Gamma$ (eV) |
|---|---|---|---|---|
| 5.3 | 1.43 | 80.9 | 4.30 | 0.33 |
| | (0.11) | (3.7) | (0.01) | (0.01) |
| 70 | 1.44 | 80.8 | 4.30 | 0.33 |
| | (0.10) | (3.6) | (0.01) | (0.01) |
| 100 | 1.45 | 80.4 | 4.29 | 0.33 |
| | (0.10) | (3.6) | (0.01) | (0.01) |
| 150 | 1.48 | 79.5 | 4.28 | 0.33 |
| | (0.10) | (3.5) | (0.01) | (0.01) |
| 200 | 1.53 | 77.3 | 4.26 | 0.33 |
| | (0.09) | (3.3) | (0.01) | (0.01) |
| 250 | 1.59 | 74.9 | 4.24 | 0.32 |
| | (0.09) | (3.2) | (0.01) | (0.01) |
| 300 | 1.68 | 71.0 | 4.20 | 0.33 |
| | (0.08) | (2.8) | (0.01) | (0.01) |

[a] Note that the thickness of the film was fixed to 258 nm at room temperature and the 90% reliability of the fitting parameters is given in parentheses.

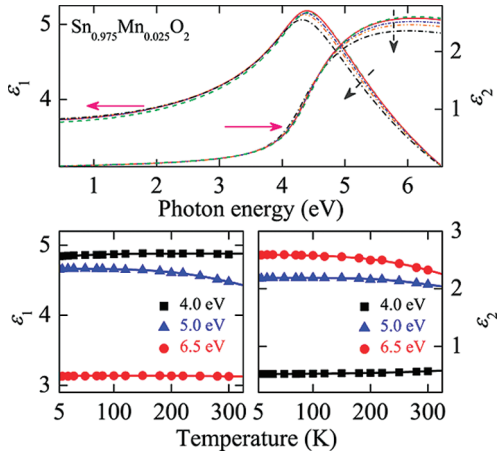


**FIGURE 7. (Top) Dielectric functions of the film doped with 2.5% Mn at the temperatures of 5.3, 150, 200, 250, and 300 K, respectively. The dash arrow indicates the temperature increases from 5.3 to 300 K. (Bottom) Variation of the dielectric functions $\varepsilon_1$ (left) and $\varepsilon_2$ (right) with temperature for three photon energies of 4.0, 5.0, and 6.5 eV, respectively. The solid lines are used to guide the eyes.**

exhibits similar behavior to the OBG, decreases with increasing temperature. With further increasing photon energy, the $\varepsilon_1$ and $\varepsilon_2$ values are significantly affected by the temperature and show a decreasing trend with increasing temperature. This is because the OBG of the film has a negative temperature coefficient and becomes narrower with increasing temperature. Therefore, the incident photons will likely excite electrons from the valence band to the conduction band and result in the strong absorption at the photon energies above the band gap, which can induce a lower dielectric function with the temperature. The bottom panel of Figure 7 shows the real part (a) and imaginary part (b) of dielectric functions with the temperature at the photon energy of 4.0, 5.0, and 6.5 eV, respectively. With increasing temperature, the dielectric functions slightly increase at the photon energy of 4.0 eV and decrease at the photon energy of 5.0 eV. However, at the photon energy of 6.5 eV, the $\varepsilon_1$ value is kept as a constant and the $\varepsilon_2$ value obviously

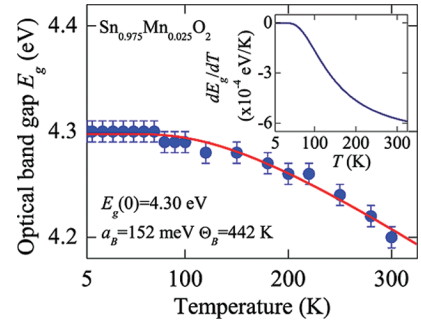


**FIGURE 8. Temperature dependence of the OBG for the film doped with 2.5% Mn. The fitting result using the Bose–Einstein model is plotted with the solid line. The inset shows the OBG narrowing coefficient.**

decreases with the temperature. It could be ascribed to the fact that the electronic band structure is generally modified corresponding to the temperature, which can affect the occupying probability of electrons and holes on the energy bands.

**Effect of Temperature on the Optical Band Gap for the $Sn_{0.975}Mn_{0.025}O_2$ Film.** The temperature dependence of the band gap energy from the interband transitions can provide important information about the electron–phonon interactions and collective excitations (39). It may be inaccurate to determine the OBG by conventional linear extrapolated method because of the small shift of the absorption edge. Fortunately, the OBG with the temperature can be directly determined by theoretical fitting to the experimental spectra by the Adachi'model. As can be seen from the Table 2, the OBG value decreases from 4.30 to 4.20 eV, corresponding to increasing the temperature from 5.3 to 300 K, which indicates that the total shift value of the OBG is about 100 meV. The value is larger than that reported on ZnO (60 meV) and GaMnN (80 meV) while less than that from AlN (150 meV) (36, 37, 40). The observed decrease in $E_g$ with the temperature can be described using the Bose–Einstein model (19, 39), in which the carrier-phonon coupling is taken into account, and can be given as

$$E_g(T) = E_g(0) - \frac{2a_B}{\exp\left(\frac{\Theta_B}{T}\right) - 1} \qquad (4)$$

Where $E_g(0)$ represents the OBG energy toward 0 K, $a_B$ is the strength of the electron–phonon interaction, $\Theta_B \equiv \hbar w / k_B$ is the characteristic temperature representing the effective phonon energy on the temperature scale, and $T$ is the experimental temperature. As shown in Figure 8, the simulated curve can agree well with the experimental data. The fitting result indicates that the $E_g(0)$ value is about 4.30 eV. The parameters $a_B$ and $\Theta_B$ in eq 4 are 152 meV and 442 K, respectively. These values are less than the data from other wide band gap materials, such as GaN (158 meV and 564 K) and AlN (670 meV and 1000 K). Furthermore, the $a_B$ value is about two times larger than that from ZnO (80 meV) (41). It reveals that the longitudinal optical phonon replicas of the

exciton transition are expected to be enhanced in $SnO_2$:Mn than in ZnO (39). The band gap narrowing coefficient of the $Sn_{0.975}Mn_{0.025}O_2$ film obtained by the formula $\alpha = dE_g/dT$ is plotted in the inset of Figure 8. The coefficient is calculated to be about $-5.74 \times 10^{-4}$ eV/K at RT. The negative $\alpha$ value indicates that the relative position of the valence band and the conduction band shifts with increasing the temperature (42). It is widely recognized that the shrinkage in the OBG with the temperature can be ascribed to the change in the band structure of the system. With increasing temperature, the lattice constant changes because of the dilatation of lattice and the shortening of interatomic distances. The variation of the lattice constant results in the modification of energy band structure, which further move the conduction band downward and the valence band upward (40, 42, 43). In addition, the OBG decreasing might also arise from the width of energy band, the electron−phonon interaction, and/or electron−lattice interaction with temperature (41−43).

## 4. CONCLUSIONS

In summary, the Mn doping dependence of dielectric functions in the $SnO_2$:Mn films has been determined from UV to NIR photon energy region by fitting the transmittance spectra with the Adachi's dielectric function model. The refractive index in the transparent region can be well-expressed by the single-oscillator model. It is found that the OBG energy shows a linearly decreasing trend with the $C_{Mn}$. The transmittance spectra of the $Sn_{0.975}Mn_{0.025}O_2$ film from 5.3 to 300 K have been measured for temperature-dependence studies. It was found that the absorption edge is strongly affected by the temperature. Moreover, the fitting results of the spectra indicate that the dielectric function values at the photon energies above band gap show a different variation trend with the temperature. The OBG of the $SnO_2$:Mn films has a negative temperature coefficient and abides by the Bose−Einstein rule. The present results might be essential for the realization of $SnO_2$-based optoelectronic and spinelectronic devices.

**Acknowledgment.** This work was financially supported by Natural Science Foundation of China (Grant 60906046), Major State Basic Research Development Program of China (Grants 2007CB924901 and 2007CB924902), Program of New Century Excellent Talents, MOE (Grant NCET-08-0192), Shanghai Municipal Commission of Science and Technology Project (Grant 10DJ1400201, 08JC1409000, 08520706100, and 09ZZ42), and the Fundamental Research Funds for the Central Universities.

### REFERENCES AND NOTES

(1) Kimura, H.; Fukumura, T.; Kawasaki, M.; Inaba, K.; Hasegawa, T.; Koinuma, H. *Appl. Phys. Lett.* **2002**, *80*, 94.
(2) Gopinadhan, K.; Kashyap, S. C.; Pandya, D. K.; Chauhary, S. *J. Appl. Phys.* **2007**, *102*, 113513.
(3) Kim, H. S.; Bi, L.; Dionne, G. F.; Ross, C. A. *Phys. Rev. B* **2008**, *77*, 214436.
(4) Wang, X. L.; Dai, Z. X.; Zeng, Z. *J. Phys.: Condens. Matter* **2008**, *20*, 045214.
(5) Xiao, Y. H.; Ge, S. H.; Xi, L.; Zuo, Y. L.; Zhou, X. Y.; Zhang, B. M.; Zhang, L.; Li, C. X.; Han, X. F.; Wen, Z. C. *Appl. Surf. Sci.* **2008**, *254*, 7459.
(6) Sharma, P.; Gupta, A.; Rao, K. V.; Owens, F. J.; Sharma, R.; Ahuja, R.; Guillen, J. M. O.; Johansson, B.; Gehring, G. A. *Nat. Mater.* **2003**, *2*, 673.
(7) Matsumoto, Y.; Murakami, M.; Shono, T.; Hasegawa, T.; Fukumura, T.; Kawasaki, M.; Ahmet, P.; Chikyow, T.; Koshihara, S.; Koinuma, H. *Science* **2001**, *291*, 854.
(8) Dietl, T.; Ohno, H.; Matsukura, F.; Cibert, J.; Ferrand, D. *Science* **2000**, *287*, 1019.
(9) Liu, S. J.; Liu, C. Y.; Juang, J. Y.; Fang, H. W. *J. Appl. Phys.* **2009**, *105*, 013928.
(10) Hu, Z. G.; Li, Y. W.; Zhu, M.; Zhu, Z. Q.; Chu, J. H. *Appl. Phys. Lett.* **2008**, *92*, 081904.
(11) Ogale, S. B.; Choudhary, R. J.; Buban, J. P.; Lofland, S. E.; Shinde, S. R.; Kale, S. N.; Kulkarni, V. N.; Higgins, J.; Lanci, C.; Simpson, J. R.; Browning, N. D.; Das Sarma, S.; Drew, H. D.; Greene, R. L.; Venkatesan, T. *Phys. Rev. Lett.* **2003**, *91*, 077205.
(12) Sun, X. Q.; Long, R.; Cheng, X. F.; Zhao, X.; Dai, Y.; Huang, B. B. *J. Phys. Chem. C* **2008**, *112*, 9861.
(13) Bouaine, A.; Brihi, N.; Schmerber, G.; Ulhaq-Bouillet, C.; Colis, S.; Dinia, A. *J. Phys. Chem. C* **2007**, *111*, 2924.
(14) Li, W. W.; Hu, Z. G.; Wu, J. D.; Sun, J.; Zhu, M.; Zhu, Z. Q.; Chu, J. H. *J. Phys. Chem. C* **2009**, *113*, 18347.
(15) Hu, Z. G.; Li, Y. W.; Yue, F. Y.; Zhu, Z. Q.; Chu, J. H. *Appl. Phys. Lett.* **2007**, *91*, 221903.
(16) Ghosh, C. K.; Malkhand, S.; Mitra, M. K.; Chattopadhyay, K. K. *J. Phys. D: Apply. Phys.* **2008**, *41*, 245113.
(17) Li, W. W.; Hu, Z. G.; Li, Y. W.; Zhu, M.; Zhu, Z. Q.; Chu, J. H. *ACS Appl. Mater. Interfaces* **2010**, *2*, 896.
(18) Ghosh, G. *Appl. Phys. Lett.* **1995**, *66*, 3570.
(19) Viña, L.; Logothetidis, S.; Cardona, M. *Phys. Rev. B* **1984**, *30*, 1979.
(20) Yoshimoto, M.; Yamamoto, H.; Huang, W.; Harima, H.; Saraie, J.; Chayahara, A.; Horino, Y. *Appl. Phys. Lett.* **2003**, *83*, 3480.
(21) Park, Y. R.; Kim, K. J. *J. Appl. Phys.* **2003**, *94*, 6401.
(22) Shen, Y. Q.; Hu, W.; Zhang, T. W.; Xu, X. F.; Sun, J.; Wu, J. D.; Ying, Z. F.; Xu, N. *Mater. Sci. Eng., A* **2008**, *473*, 201.
(23) Hu, Z. G.; Li, W. W.; Wu, J. D.; Sun, J.; Shu, Q. W.; Zhong, X. X.; Zhu, Z. Q.; Chu, J. H. *Appl. Phys. Lett.* **2008**, *93*, 181910.
(24) Heaven, O. S. *Optical Properties of Thin Solid Films*; Dover: NewYork, 1991; Chapter 4, p 69.
(25) Djurišić, A. B.; Chan, Y.; Li, E. H. *Mater. Sci. Eng., R* **2002**, *38*, 237.
(26) Adachi, S. *Phys. Rev. B* **1987**, *35*, 7454.
(27) Adachi, S. *Phys. Rev. B* **1988**, *38*, 12345.
(28) Hu, Z. G.; Huang, Z. M.; Lai, Z. Q.; Wang, G. S.; Chu, J. H. *Thin Solid Films* **2003**, *437*, 223.
(29) Palik, E. D. *Handbook of Optical Constants of Solid*; Academic: Orlando, FL, 1985.
(30) Hu, Z. G.; Weerasekara, A. B.; Dietz, N.; Perera, A. G. U.; Strassburg, M.; Kane, M. H.; Asghar, A.; Ferguson, I. T. *Phys. Rev. B* **2007**, *75*, 205320.
(31) Tang, H.; Lévy, F.; Berger, H.; Schmid, P. E. *Phys. Rev. B* **1995**, *52*, 7771.
(32) Cardona, M. *Phys. Rev.* **1965**, *140*, A651.
(33) The dielectric function is taken from the optical constant database of spectroscopic ellipsometry software provide by SC630UVN by Shanghai Sanco Instrument, Co., Ltd.
(34) Ke, C.; Zhu, W.; Pan, J. S.; Karamat, S. *J. Appl. Phys.* **2010**, *107*, 013515.
(35) Mishra, K. C.; Johnson, K. H.; Schmidt, P. C. *Phys. Rev. B* **1995**, *51*, 13972.
(36) Chen, N. B.; Wu, H. Z.; Qiu, D. J.; Xu, T. N.; Chen, J.; Shen, W. Z. *J. Phys.: Condens. Matter* **2004**, *16*, 2973.
(37) Tang, X.; Hossain, F.; Wongchotigul, K.; Spencer, M. G. *Appl. Phys. Lett.* **1998**, *72*, 1501.
(38) Kaldis, E. *Current Topics in Materials Science*; North-Holland: Amsterdam, 1981; Vol. 7, pp 143−482.
(39) Nam, K. B.; Li, J.; Lin, Y.; Jiang, H. X. *Appl. Phys. Lett.* **2004**, *85*, 3489.
(40) Guo, L. L.; Shen, W. Z.; Zhang, Y. H. *J. Appl. Phys.* **2006**, *99*, 113533.
(41) Saha, S.; Mehan, N.; Sreenivas, K.; Gupta, V. *Appl. Phys. Lett.* **2009**, *95*, 071106.
(42) Yakuphanoglu, F.; Arslan, M.; Küçükislamoğlu, M.; Zengin, M. *Sol. Energy* **2005**, *79*, 96.
(43) Li, B. S.; Liu, Y. C.; Zhi, Z. Z.; Shen, D. Z.; Lu, Y. M.; Zhang, J. Y.; Fan, X. W. *J. Cryst. Growth* **2002**, *240*, 479.

AM100353F